Fuel 304 (2021) 121445

Contents lists available at ScienceDirect

Fuel

journal homepage: www.elsevier.com/locate/fuel

Full Length Article

Alkali metal-resistant mechanism for selective catalytic reduction of nitric oxide over V_2O_5/HWO catalysts

Running Kang [a,b], Junyao He [a], Feng Bin [a,b,*], Baojuan Dou [c], Qinglan Hao [c], Xiaolin Wei [a,b], Kwun Nam Hui [d], Kwan San Hui [e,*]

[a] State Key Laboratory of High-Temperature Gas Dynamics, Institute of Mechanics, Chinese Academy of Sciences, Beijing 100190, PR China
[b] School of Engineering Science, University of Chinese Academy of Sciences, Beijing 100049, PR China
[c] Tianjin University of Science & Technology, Tianjin 300457, PR China
[d] Institute of Applied Physics and Materials Engineering, University of Macau, Avenida da Universidade, Taipa Macau, P.R. China
[e] School of Engineering, Faculty of Science, University of East Anglia, Norwich Research Park NR4 7TJ, United Kingdom

ARTICLE INFO

Keywords:
Commercial bacterial cellulose
V_2O_5/HWO catalyst
Alkali metal-resistant
Poisoning
SCR reaction

ABSTRACT

A series of V_2O_5/HWO catalysts are prepared by hydrothermal and impregnation methods using different precursors, among which the V_2O_5/HWO-C catalyst exhibited the optimal NH_3-SCR performance. Compared to oxalic acid (O) and water (W), commercial bacterial cellulose (C) as a precursor can firstly achieve a more controllable synthesis to form hexagonal WO_3 (HWO) of V_2O_5/HWO-C catalyst. Various characterization (XRD, N_2-BET, TEM, SEM, XPS, EDX mapping, and NH_3/NO-TPD-MS) indicate that a higher specific surface area, abundant active oxygen and surface acidity result from the V_2O_5/HWO-C catalyst. The reason is that HWO-C has an excellent and smooth rod-shaped morphology, which promotes high dispersion of V_2O_5 on its surface. In situ IR results show that the SCR follows the Langmuir-Hinshelwood (L-H) mechanism, where absorbed NO_x intermediate species are formed on the V_2O_5 and react with the NH_4^+ and NH_{3abs} groups of V_2O_5 and HWO. After loading 1.75 wt% K^+, the obtained K-V_2O_5/HWO-C catalyst exhibits effective resistance to K poisoning and SO_2, and retains 78 % NO_x conversion efficiency at 360 °C after 10 h, attributed to the effective capture of K^+ (1.04 wt %) in HWO-C channels via a new pathway, although approximately 0.71 wt% K^+ are located on HWO-C external surface with weak bonding to V_2O_5.

1. Introduction

The selective catalytic reduction (SCR) of NO_x by NH_3 is deemed as an effective strategy for controlling NO_x emissions in flue gas from fuel combustion[1-4]. The poisoning effect of alkali metals on SCR catalysts, however, is often substantially induced by the combustion of high alkaline solid fuel[56]. As the core of this technology for denitration ($deNO_x$), methods for the synthesis of alkali-resistant catalysts, including those with different active components and diverse preparation methods, have been greatly developed over the past two decades [7,8]. The deactivation and resistant deactivation mechanisms of catalysts by alkali metals for SCR processing have garnered much attention and have been extensively studied[9-13].

The preparation of vanadium-based SCR catalysts, as a significant design step to realize alkali metal resistance, has both scientific and applied interest. This procedure is crucial for understanding controllable structure synthesis using various precursors to enhance catalytic performance in surficial reactions. Bacterial cellulose as a precursor can be employed instead of the typically used oxalic acid since this inexpensive and green biobased material possesses a three-dimensional network structure and abundant hydroxyl groups that promote nucleation and binding for metal oxide particles. Previously, researchers reported that La_2CuO_4 nanocrystals synthesized by bacterial cellulose nanofibre templates exhibit considerable activity for methanol steam reforming, arising from their unique structure and large specific area [14]. Nevertheless, there is limited statistical evidence related to the morphologically controllable synthesis of $deNO_x$ catalysts using different precursors, and the predominant contributor to the enhanced activity has not yet been reported.

V_2O_5-WO_3-TiO_2 prepared by an oxalic acid precursor, as a traditional

* Corresponding authors at: State Key Laboratory of High-Temperature Gas Dynamics, Institute of Mechanics, Chinese Academy of Sciences, Beijing 100190, PR China (F. Bin).
E-mail addresses: binfeng@imech.ac.cn (F. Bin), k.hui@uea.ac.uk (K. San Hui).

https://doi.org/10.1016/j.fuel.2021.121445
Received 12 January 2021; Received in revised form 6 June 2021; Accepted 12 July 2021
Available online 23 July 2021

and commercial deNO$_x$ catalyst, is commonly employed owing to its excellent catalytic properties [2,15,16]. Lian et al reported that the V_2O_5/TiO_2 catalyst with high rutile phase content exhibited superior NH_3-SCR catalytic performance [17]. Unfortunately, the catalyst is easily deactivated in flue gas containing alkali metals. Deng et al. [18] pointed out that upon the addition of various alkali metals, the activity of the V_2O_5-WO_3-TiO_2 catalyst was greatly inhibited by K and Na (in decreasing order) due to the decreasing specific surface area and the masking of V_2O_5. Kong et al suggested that the deactivation rate of potassium-poisoned catalysts follows KCl > K_2O > K_2SO_4 in the SCR reaction over the V_2O_5-WO_3-TiO_2 catalyst[19]. Although supported $V_2O_5 - WO_3/TiO_2$ catalysts have not been extensively examined for the interaction between TiO_2, V_2O_5 and alkali metals, some publications imply that the nature of the supported vanadium oxide sites depends on the specific precursors and preparation methods[20-23], but these claims were not given by supporting information. Recently, several successful attempts have been made to improve the alkali metal-resistant performance of vanadium oxide catalysts [24]. According to Hu et al. and Huang et al. [23,25], MnO_2 and WO_3 prepared by oxalic acid as precursors can effectively trap alkali metal ions and prevent V_2O_5 poisoning during SCR due to the structure of MnO_2 and WO_3. Further, the Zheng et al. proposed self-protect mechanism via alkali-trapping of HWO rather than including alkali-blocking of V_2O_5 in the SCR process over V_2O_5/HWO catalyst using oxalic acid precursor [26]. Despite previous studies concerning deactivation and resistant deactivation models of alkali metals in the SCR reaction, the exact distribution of alkali metal species with quantitative or semi quantitative analysis on the catalyst leading to the alkali metal-resistant mechanism remains unclear.

In this investigation, a series of V_2O_5/HWO catalysts are prepared by three different precursors, including commercial bacterial cellulose, oxalic acid and water, to study the interactions among the morphological characteristics and the catalytic activity in the SCR reaction. In particular, the alkali metal-resistant pathways for the distribution of alkali metal ions (K^+) on the catalyst and V_2O_5/HWO-C were proposed in detail via X-ray diffraction (XRD), transmission electron microscopy (TEM), energy-dispersive X-ray spectroscopy (EDX) mapping, X-ray photoelectron spectroscopy (XPS) and in situ infrared (in situ IR) analysis. The results obtained will provide new insights into the design of advanced catalysts and the corresponding alkali metal-resistant mechanisms for SCR reactions.

2. Experimental specifications

2.1. Catalyst preparation

To investigate the relationship between the porous structure and activity, HWO was prepared by a hydrothermal method using different pore-forming agents, including commercial bacterial cellulose (C), oxalic acid (O) and water (W). The $(NH_4)_{10}W_{12}O_{41} \sim xH_2O$ (2.13 g), $(NH_4)_2SO_4$ (8.32 g) and pore-forming materials (2.10 g) were dissolved in deionized H_2O (80 mL). The homogeneous solution was kept at 180 °C for 12 h in an autoclave (200 mL) and then washed with deionized H_2O, followed by drying at 120 °C. The theoretical support content of V_2O_5 is 10% in the all catalysts. The obtained catalysts were denoted as HWO-C, HWO-O and HWO-W. The V_2O_5/HWO catalysts were synthesized by wet impregnation of the various HWO with NH_4VO_3 solutions. The resulting solutions were stirred and evaporated at 80 °C for 0.5 h, and then they were calcined at 400 °C for 4 h to obtain V_2O_5/HWO-C, V_2O_5/HWO-O and V_2O_5/HWO-W catalysts. The K in gas phase is always absorbed and migrated on the catalyst in the flue gas. Therefore, considering that the deactivation of the catalyst by alkali metals in off-gas is a long-term process, the alkali resistance of the samples was simulated by immersing method and to realize extreme condition of K loading and poisoning. To study the actual deactivation as well as the capture of K^+ via the catalyst surface morphology and channels for the SCR reaction, a KCl (0.03 g) aqueous solution was loaded with stirring onto the V_2O_5/HWO-C (1 g) catalyst and dried at 120 °C for 4 h to obtain K-V_2O_5/HWO-C. The schematic diagram describing the catalysts preparation is shown in Fig. 1. The metal content in the catalysts was detected by X-ray fluorescence (XRF) and is shown in Table 1.

2.2. Characterization

The elemental composition of the catalysts was obtained by XRF with a Power 4200 scanning XRF spectrometer. The textural properties were investigated by N_2 adsorption–desorption (N_2-Brunauer, Emmett and Teller, N_2-BET) at the liquid nitrogen temperature using a 16 Autosorb-Iq-MP instrument (Quantachrome). XRD patterns were measured by an XD-3-automatic (PERSEE) equipped with a Cu Kα radiation source (λ = 0.1541 nm). Rietveld refinement analyses of the XRD data profiles were subsequently performed by using TOPAS Academic and Fullprof software package. The morphology and distribution of surface elements were determined by TEM (JEM 2100F, Oxford) equipped with EDX mapping (Tecnai G^2 F20, Oxford). Temperature-programmed reduction (H_2-TPR) was conducted on a TP5080B chemisorption analyzer with approximately 50 mg of each example. Each sample was pretreated at 300 °C for 0.5 h in a flow of N_2 (50 mL/min). The temperature was increased from room temperature to 900 °C at a heating rate of 10 °C/min in a flow of a H_2 (30 mL/min), and the H_2 consumption was recorded continuously by the TCD detector. Temperature-programmed NH_3 desorption (NH_3-TPD-TCD) experiments were performed using a TP5080B chemisorption analyser with 5 vol% NH_3/Ar (50 mL/min) at a heating rate of 10 °C/min from 100 °C to 800 °C. The absorbed gases were passed through the samples for 1 h at 100 °C and started desorption to maintain stable NH_3 absorption and avoid the signal interference. Temperature-programmed desorption of NO, and NH_3 (NO– and NH_3-TPD-MS) was also conducted by same analyzer, monitored by an online quadrupole mass spectrometer (MS, Pfeiffer Omnistar^{TM}). After being pretreated at 300 °C under flowing helium (50 mL/min) for 1 h, the powder sample (20 mg) was cooled to 50 °C and then adsorbed to saturation by 5 vol% NO/He, or 5 vol% NH_3/He for 0.5 h. The desorption signals were recorded from 50 °C to 1000 °C at an increasing rate of 10 °C/min. For the chemical states of surface elements, XPS was carried out with a Kratos Axis Ultra DLD spectrometer. The binding energy of surface elements was calibrated with C1s (284.8 eV) peak. In situ IR spectroscopy was recorded with a Bruker Tensor 27 spectrophotometer with a self-designed magnetically driven transmission cell. Prior to obtaining each IR spectrum, the sample (20 mg) was pretreated under N_2 flow with 100 mL/min at 400 °C to remove adsorbed impurities. The spectra were recorded by accumulating 32 scans at a heating rate of 10 °C/min to 500 °C after the absorption of reactants for 0.5 h.

2.3. Catalytic activity testing

The SCR activity test was evaluated under atmospheric pressure in a fixed-bed quartz tube reactor (i.d. = 4 mm). The catalyst (200 mg, 0.1–0.15 mm) was charged for each test. The feed gases contained 300 ppm NO, 300 ppm NH_3, 5 vol% O_2 and N_2 as the balance gas with a total flow rate of 200 mL/min, corresponding to a gas hourly space velocity (GHSV) of 170,000 h^{-1}. Temperature-programmed catalytic reduction of NO was performed under heating (10 °C/min) from room temperature to 400 °C, and a K-type thermocouple was positioned between the reactor and oven wall to monitor the oven temperature. The concentrations of NO, NH_3, SO_2 and O_2 were measured by an online multi-component analyser (Gasboard-300UV for NO (±2%FS) /NH_3 (±4%FS) /O_2 (±3%FS), and Gasboard-300plus for SO_2 (±2%FS), Hubei Cubic-Ruiyi Instrument Co., Ltd.). Good reproducibility of catalysts was found for each SCR experiment at three times.

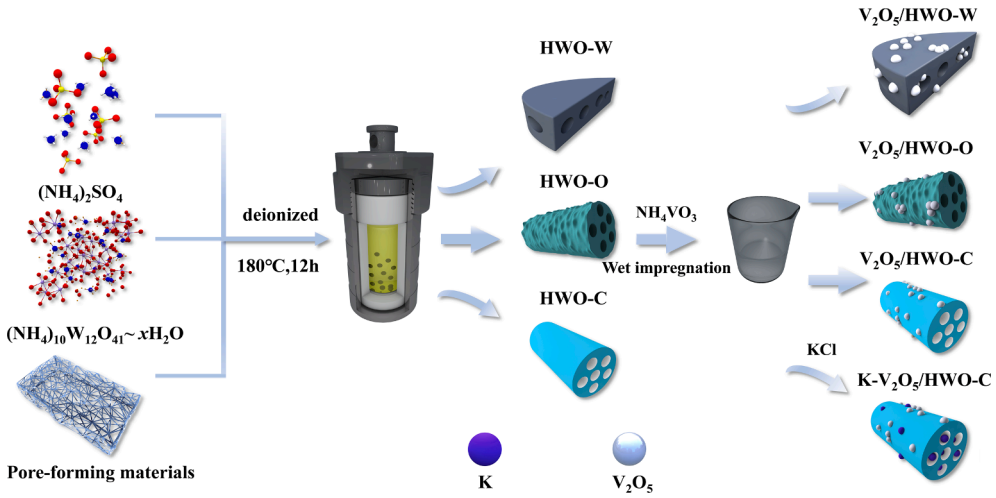

Fig. 1. Schematic diagram of the catalysts preparation.

Table 1
The element content by XRF and the atomic content by XPS of the catalysts.

Samples	V_2O_5 (%)	WO_3 (%)	K/K_2O (wt%)	$(V^{5+}+V^{4+})/V_{total}$
V_2O_5/HWO-W	10.05	89.95	–	0.980
V_2O_5/HWO-O	10.02	89.98	–	0.971
V_2O_5/HWO-C	9.87	90.13	–	0.937
K-V_2O_5/HWO-C	9.74	88.51	1.75	0.952

3. Results and discussion

3.1. Structure, morphology and occurrence state

Fig. 2 displays the XRD patterns of the V_2O_5/HWO-W, V_2O_5/HWO-O, V_2O_5/HWO-C and K-V_2O_5/HWO-C catalysts. Apart from the strong characteristic diffraction peaks of hexagonal WO_3 for all the catalysts (PDF#75–2187), weak diffraction peaks assigned to V_2O_5 crystals (PDF#85–0601) can be observed in the spectra of V_2O_5/HWO-W, V_2O_5/HWO-O and V_2O_5/HWO-C. The size of HWO channels is not large enough to accommodate V_2O_5 particles[25], so that V_2O_5 is dispersed on the external surface of HWO rather than being introduced into HWO channels. The only weak peaks of V_2O_5 are detected on the V_2O_5/HWO-W, V_2O_5/HWO-O and V_2O_5/HWO-C in the Fig. 2, indicating that the most vanadium species are well dispersed and correspondingly, a little part of vanadium species are formed as crystalline on the catalysts.

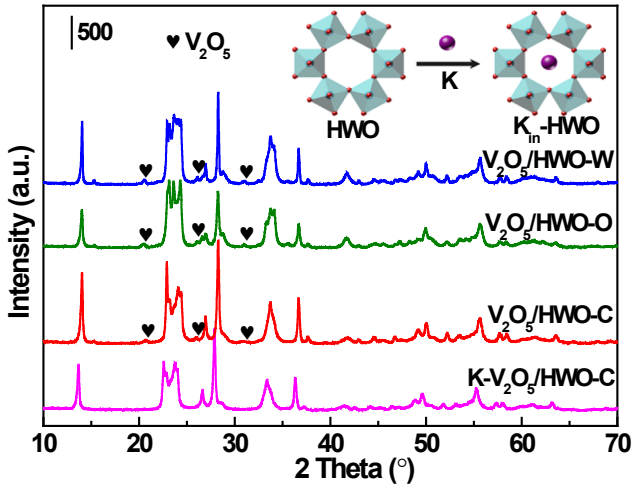

Fig. 2. XRD patterns of the catalysts.

Furthermore, Compared with V_2O_5/HWO-W and V_2O_5/HWO-O, V_2O_5/HWO-C shows relative highly dispersed states of V_2O_5 on the surface, according to the existence of much too weak peaks of V_2O_5 at 20.7° (001 plane), 25.9° (101 plane) and 31° (031 plane). After K^+ was loaded, the peak of V_2O_5 crystallites became weaker and less obvious, which means that the active component of vanadium might be covered by some K^+ on the catalyst surface [27]. Surprisingly, the shift of the diffraction peaks of HWO towards lower 2θ values for K-V_2O_5/HWO-C reveals that most K^+ ions are probably inserted into the HWO channels to cause a bigger lattice constant. The strength of HWO slightly decreases could be assigned to the some K^+ covered on the catalyst surface. A structural model of the local situation of K^+ is shown in the inset of Fig. 2.

To further confirm the K^+ position, the corresponding Rietveld XRD refinements of V_2O_5/HWO-C and K-V_2O_5/HWO-C catalysts are shown in Fig. 3. All the Bragg reflections of the K-V_2O_5/HWO-C transfer to lower angles, in comparison with the V_2O_5/HWO-C. Then the calculated lattice constants of HWO (7.2993 Å×7.2993 Å×3.8872 Å) on the V_2O_5/HWO-C exhibit an expansion of a and b axis and a contraction of c axis after K^+ insertion into the HWO tunnels (7.3088 Å×7.3088 Å×3.8807 Å) over K-V_2O_5/HWO-C (Table S1). The Rietveld refinement analyses show that the K^+ occupies exactly at the Wyckoff 1a site or the (0,0,0) site and the occupation 0.25 (Table S2), indicating that the K^+ ions are coordinated to six oxygen atoms (K-O) in the channels with a mean K-O bond length of ~ 2.68 Å [25]. Based on the typical Space group of HWO (P6/mmm), a structural model of the local region of K^+ is carried out in the inset of Fig. 3.

The N_2 adsorption–desorption isotherms are analysed to study the difference in specific surface area (SSA), pore volume and pore size over various catalysts, as shown in Fig. 4. All the catalysts show type IV isotherms with a H3-type hysteresis loop, indicating that a large number of mesopores are formed in the catalysts. Due to the abundant network structure of commercial bacterial cellulose, V_2O_5/HWO-C shows a higher SSA (11.85 m^2/g) than V_2O_5/HWO-W (4.88 m^2/g) and V_2O_5/HWO-O (8.92 m^2/g) and, therefore, promotes the dispersion of V_2O_5 on the HWO surface. Particularly, the pores (Fig. 4b) show an exclusive region with a size<5 nm for V_2O_5/HWO-C by using bacterial cellulose as pore forming materials, favouring the formation of abundant channels for HWO and the interaction between many more V_2O_5 active sites and the HWO support, thus improving the catalytic performance. It has been reported that the small size (<5nm) among the supported catalyst promotes the formation of coordinated atoms with higher chemical activity [28]. The pore volume of V_2O_5/HWO-C (0.033 cm^3/g) is approximately equal to that of K-V_2O_5/HWO-C (0.031 cm^3/g) since some K^+ is located in the channels of the K-V_2O_5/HWO-C catalyst via HWO trapping[29]. There are visible differences between V_2O_5/HWO-C and K-V_2O_5/HWO-

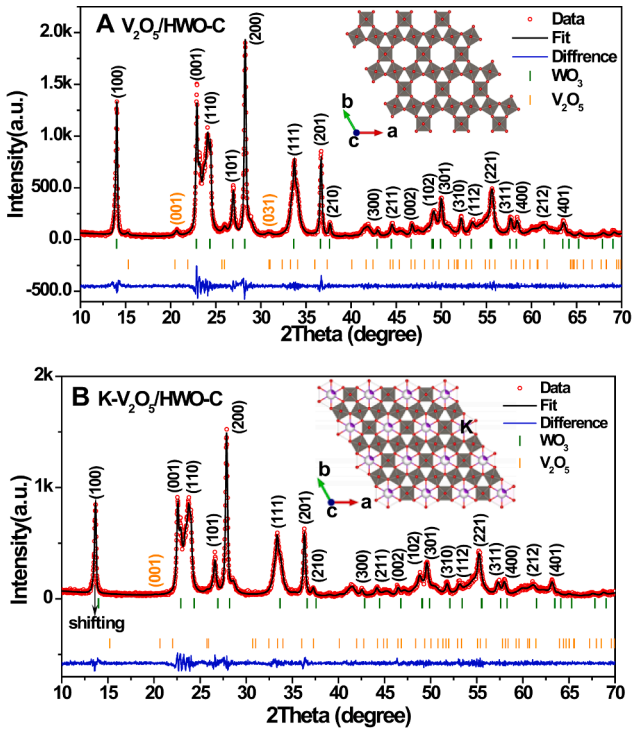

Fig. 3. XRD patterns (red lines) and corresponding Rietveld refinements (black lines) of the (A) V_2O_5/HWO-C and (B) K-V_2O_5/HWO-C. The green lines are the differential XRD pattern of the catalysts. The short vertical lines below the XRD patterns are assigned to the peak positions of all the possible Bragg reflections. (For interpretation of the references to colour in this figure legend, the reader is referred to the web version of this article.)

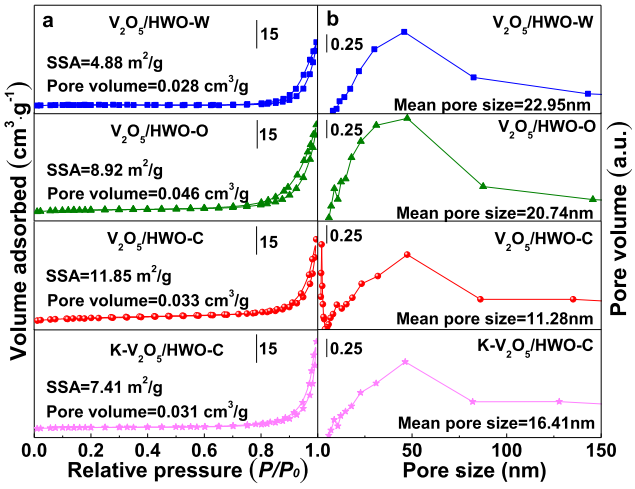

Fig. 4. N_2 adsorption–desorption isotherms (a) and pore size distribution (b) of catalysts.

C for both SSA and mean pore size. The V_2O_5/HWO-C shows a bigger SSA and a lower mean pore size than that of K-V_2O_5/HWO-C, attributed to partially K^+ leads to block the micropores entrance, and agglomeration between some K^+ and vanadium oxides causes the SSA decreasing and means pore size of accumulation pores increasing. This finding indicates that the other K^+ ions may diffuse onto the surface of the catalyst or block the entrance of HWO channels.

Representative TEM images of the catalysts are presented in Fig. 5. Among all tested catalysts, V_2O_5/HWO-C (Fig. 5c and 5 g) exhibits the best and smoothest rod-shaped morphology of HWO and a good dispersion of V_2O_5 on the surface. Commercial bacterial cellulose possesses an ultrafine three-dimensional network structure and unique properties including high crystallinity, good tensile strength, and mouldability. Therefore, the cellulose here not only promotes controllable synthesis to form a catalyst with a regular morphology but also possesses a high surface area for dispersing more metal ions, which is in agreement with the XRD and N_2-BET results. High-resolution TEM (HR-TEM) is further performed on V_2O_5/HWO-C (Fig. 5c), where a representative individual HWO rod with the side line parallel to the (1 0 0) plane is found by the fringe distance of 0.61 nm. Crystalline V_2O_5 is observed on the surface of HWO by measuring the D spacing at d = 0.29 nm. Typical morphologies with broader scales are also displayed in Fig. 5e-h. The loading of K^+ results in no visible change in the rod-shaped morphology (Fig. 5d), but some K^+ ions are found on the surface of K-V_2O_5/HWO-C. Although the HWO channels synthesized by many precursors would be about 0.54 nm and V_2O_5 nanoparticles will not be captured [30]. The size of the HWO channels is ~ 0.54 nm, which is appropriate for accommodating metal ions with ionic radii<0.17 nm [31], thus easily capturing K^+ (0.13 nm) in the many easily formed HWO channels rather than capturing V_2O_5 nanoparticles for the K-V_2O_5/HWO-C. According to the results above, there are two locations for K^+ ions: i) on the HWO external surface and ii) inside the HWO channels in a stable state.

The distribution of elements in the cross-section channel of K-V_2O_5/HWO-C catalyst have been given in Fig. 6 (a), (b) and (c). It is clear that the vanadium and part potassium species are detected on the HWO surface and the presence of the isolated individual potassium atoms. Combined with the Rietveld refinements and TEM results, these results are further confirmed thus most potassium ions are effectively captured in HWO-C channels through an ions exchange path in HWO-C channels. The hexagonal morphology of HWO-C in V_2O_5/HWO-C catalyst has been also well characterized by SEM, as shown in Fig. 6(d). It can be found that the controllable synthesis of catalytic hexagonal morphology was achieved successfully for the V_2O_5/HWO-C catalyst.

3.2. Chemical states, distribution of elements and acidity

The chemical states and surficial element compositions of the catalysts are investigated by XPS analysis. The V 2p spectra of the catalysts (Fig. 7a) show three main peaks for V^{5+} (517.1 eV), V^{4+} (516.3 eV) and V^{3+} (515.3 eV) [32]. The semiquantitative data, as listed in Table 1, give $(V^{5+}+V^{4+})$ / V_{total} ratios of 0.937 for V_2O_5/HWO-C, 0.971 for V_2O_5/HWO-O, 0.980 for V_2O_5/HWO-W and 0.952 for K-V_2O_5/HWO-C. After loading K^+ ions on the V_2O_5/HWO-C catalyst, the ratio of the lattice oxygen (O_L^{2-}) in the K-V_2O_5/HWO-C increases, and occurring the slightly change of vanadium chemical valence during the bond between V_2O_5 and partial K on the catalyst surface, hence the $(V^{5+}+V^{4+})/V_{total}$ ratios of V_2O_5/HWO-C (0.937) is lower than K-V_2O_5/HWO-C (0.952). The W 4f spectra of the catalysts (Fig. 7b) are deconvoluted into $4f_{5/2}$ and $4f_{7/2}$ spin–orbit components [7,33]. The presence of W^{6+} in the catalysts favours the formation of a strong carrier-metal interaction via electronic transitions between W^{6+} and V^{n+} [34,35]. The O 1 s curve (Fig. 7c) is fitted to two peaks corresponding to surface-adsorbed oxygen (O_a, 531.6 eV) and lattice oxygen (O_L, 530.5 eV)[36,37]. The peak of hydroxyl species is too low to fit accurately at ~ 530.8 eV due to a large peak at 530.5 eV for lattice oxygen in the catalysts. It was reported that O_a is the most active oxygen species that plays a crucial role in the SCR reaction due to its higher mobility on the catalyst surface than the inactive O_L [32]. Herein, O_a ratios are calculated by $O_a/(O_a + O_L)$ and decrease in the following order (Fig. 7c): V_2O_5/HWO-C (31.2 %) > K-V_2O_5/HWO-C (30.6 %) > V_2O_5/HWO-O (25.5 %) > V_2O_5/HWO-W (22.5 %). The high O_a ratios of V_2O_5/HWO-C and K-V_2O_5/HWO-C should be related to the abundant oxygen ions in the commercial bacterial cellulose, which promotes contact with more metal ions in the catalysts. The K 2p spectra of K-V_2O_5/HWO-C were also obtained (as shown in the Fig. S1), verifying that some K^+ ions exist on the catalyst

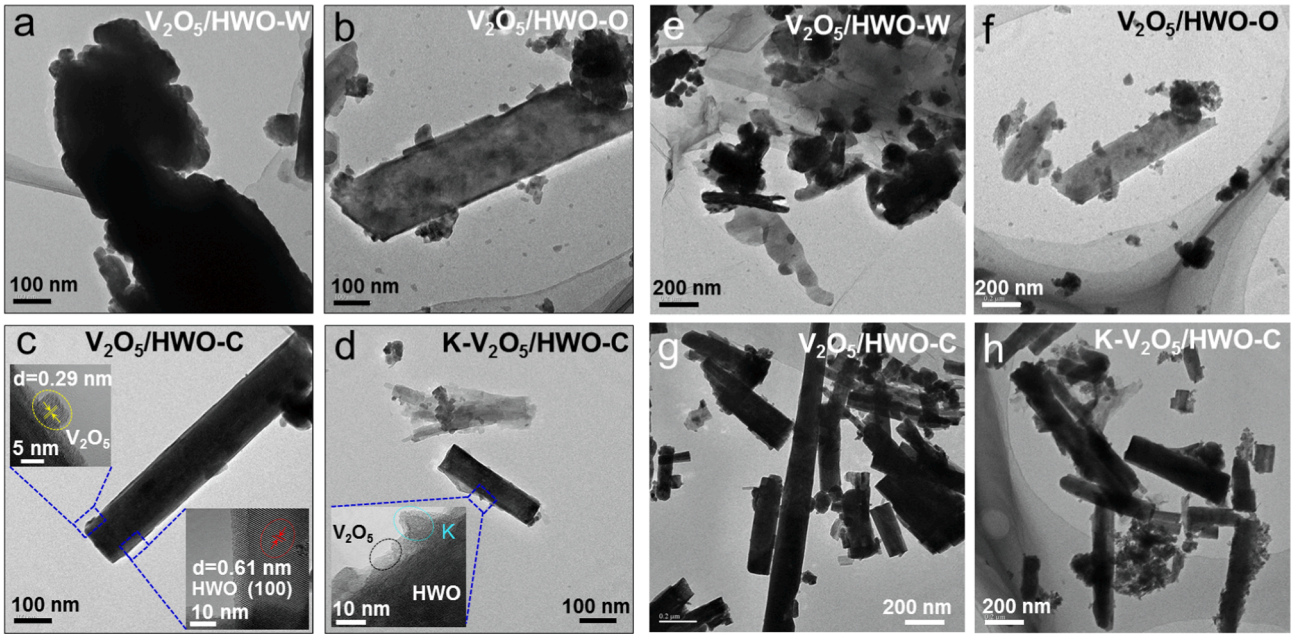

Fig. 5. TEM images of catalysts.

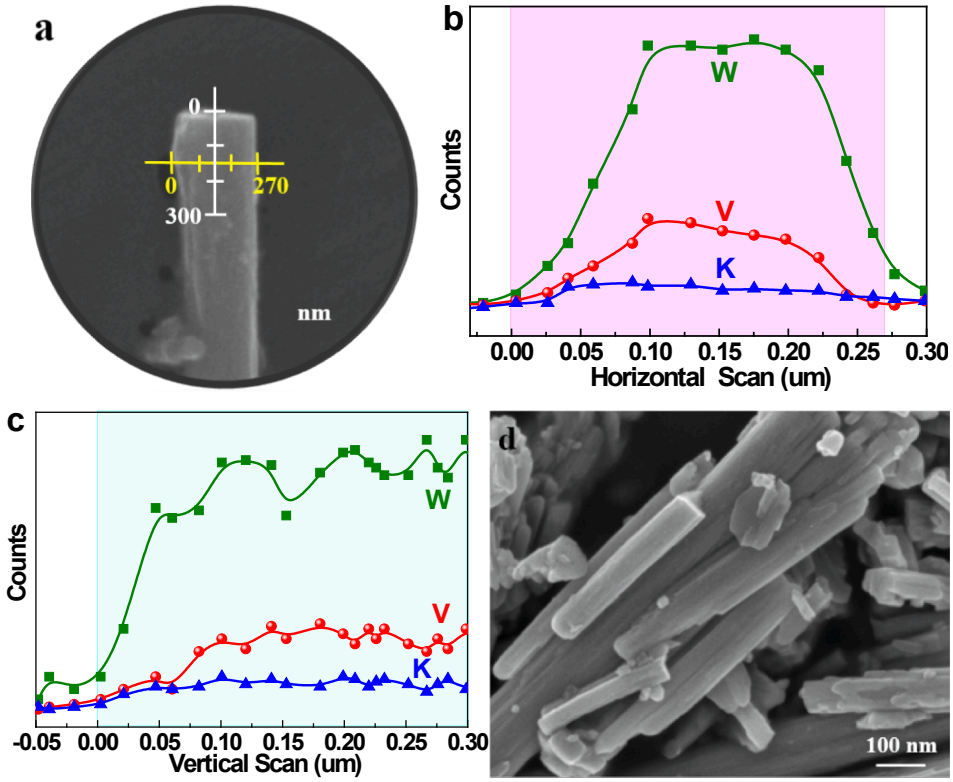

Fig. 6. (a) TEM images with line-scanned EDX spectra of the K-V_2O_5/HWO-C, (b) horizontal line-scanned, (c) vertical line-scanned, (d) SEM image of V_2O_5/HWO-C.

surface.

The redox ability of vanadium and tungsten species with different precursors and alkali metal of catalysts were investigated with H_2-TPR analysis, as shown in Fig. 8. The reduction peaks located at 610–644 °C and 730–750 °C are ascribed to reduction of $V^{5+}/V^{4+}\rightarrow V^{3+}$ and $W^{6+}\rightarrow W^0$, respectively[38]. The dispersed vanadium is considered as a key catalytic cycle for the SCR reaction due to the peak position of W species showed no obvious change in the catalysts although the content of W is far more than that of V. Compared with the peaks of vanadium on the V_2O_5/HWO-O (629 °C) and V_2O_5/HWO-W (635 °C), the V_2O_5/HWO-C shifts to lower temperature (610 °C), indicating that the well dispersed vanadium species are easily reduced and promote the activity of V_2O_5/HWO-C. This is consistent with the XRD, TEM, O_a of XPS and SCR activity results. After loading K^+ on the V_2O_5/HWO-C, the reduction peak of V species of K-V_2O_5/HWO-C shifts to higher temperatures (644 °C), attributed to partial K^+ bonds and weakens the oxidation

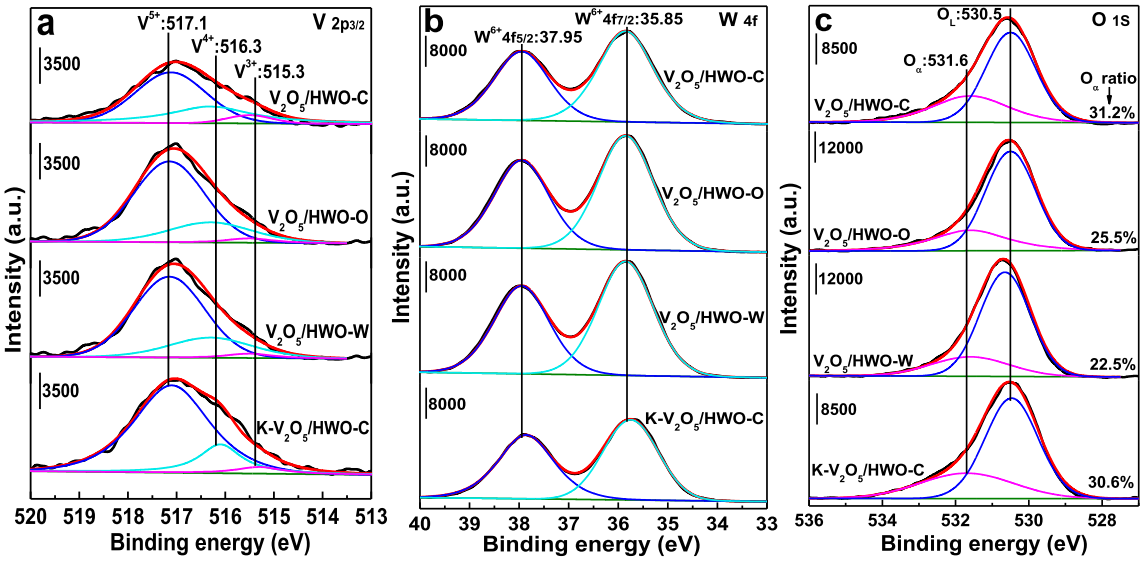

Fig. 7. XPS spectra of (a) V 2p, (b) W 4f and (c) O 1 s over the catalysts.

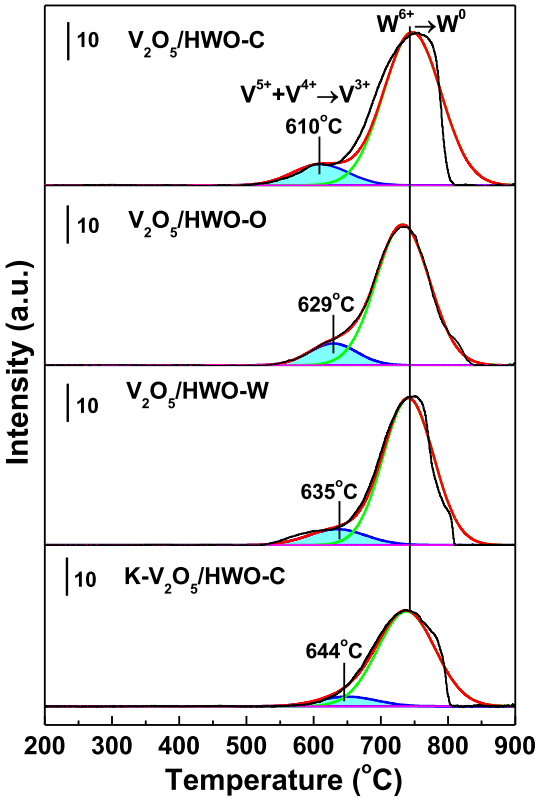

Fig. 8. H_2-TPR profiles of the catalysts.

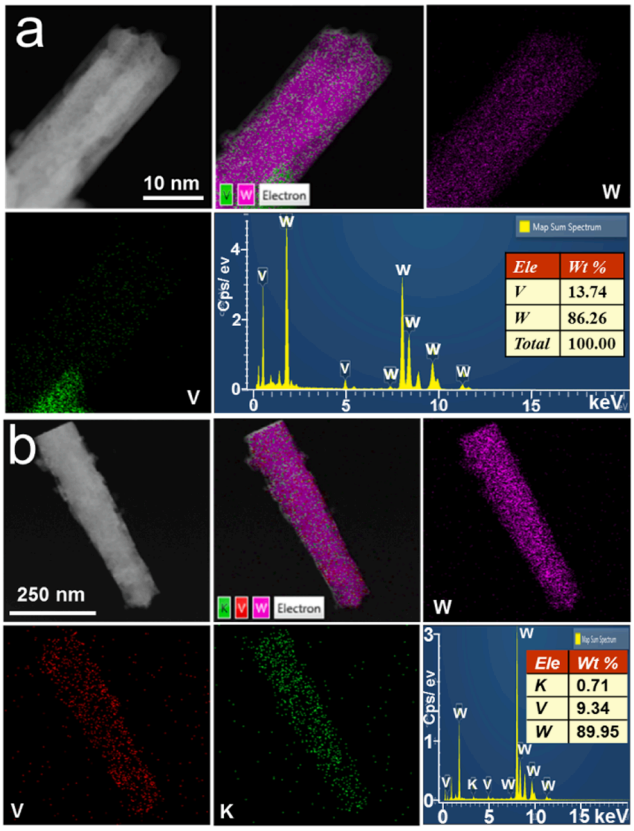

Fig. 9. TEM images, EDX mapping and spectrum of the (a) V_2O_5/HWO-C and (b) K-V_2O_5/HWO-C catalysts.

activity of V species [39]. Further the peak intensity of W species for K-V_2O_5/HWO-C become lower than that of V_2O_5/HWO-C, suggesting that the captured K^+ in HWO channel has a stronger interaction with oxygen in tungsten oxides.

The potassium element loaded on the whole regular K-V_2O_5/HWO-C rod would have an effect on the SCR activity. The TEM images, corresponding EDX maps and semiquantitative analysis of V_2O_5/HWO-C and K-V_2O_5/HWO-C are shown in Fig. 9, which illustrate the spatial distribution and high dispersion of vanadium and potassium on the catalyst surface. The vanadium and potassium species are well dispersed on the HWO external surface. There are three possible locations for K^+ ions: i) on the HWO external surface not in conjunction with V_2O_5, ii) on the HWO external surface in conjunction with V_2O_5, and iii) at the entrance into the HWO channels. Based on the N_2-BET results, the mean pore size of K-V_2O_5/HWO-C (16.31 nm) is higher than that of V_2O_5/HWO-C (11.28 nm). The increase in the mean pore size is responsible for the partial number of K^+ ions making contact with V_2O_5 to form relatively large particles on the catalyst surface, possibly resulting in a decrease in the catalyst activity in the SCR reaction, which can be confirmed by the SCR activity in Fig. 12. Therefore, the locations of K^+ should be

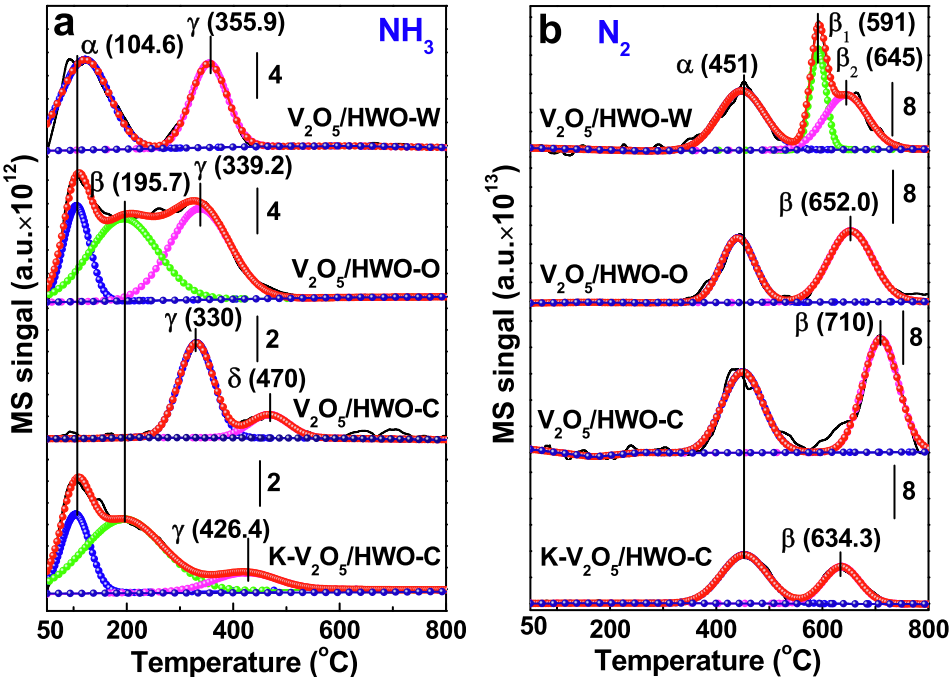

Fig. 10. NH_3-TPD-MS (a) NH_3 and (b) N_2 profiles of the catalysts.

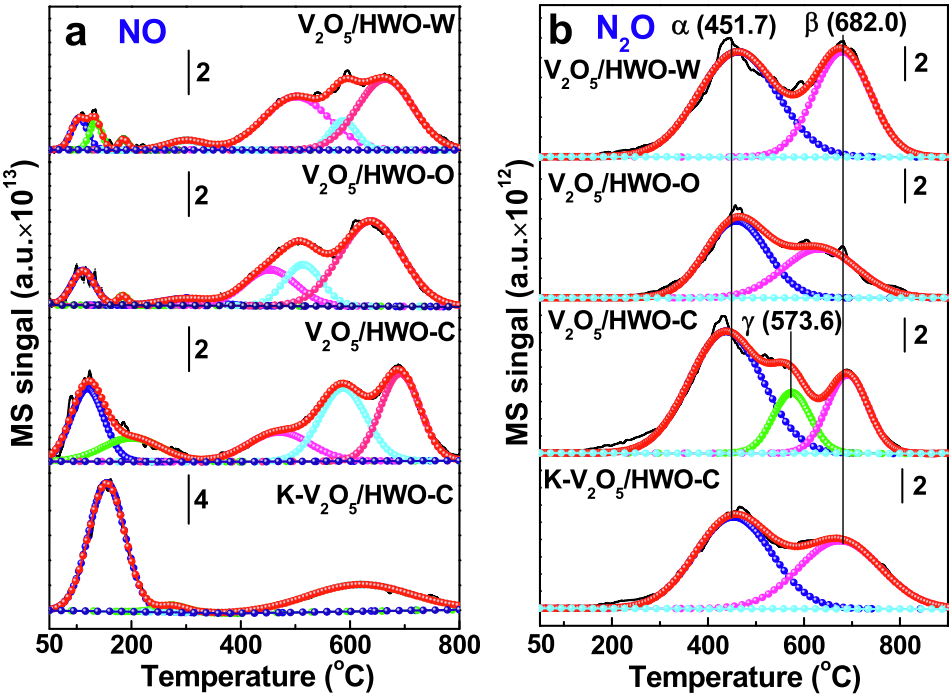

Fig. 11. NO-TPD-MS (a) NO and (b) N_2O profiles of the catalysts.

determined in the last two forms as discussed above. The obtained contents of tungsten and vanadium elements are also similar to the XRF results for typical K-V_2O_5/HWO-C rod (big scale at 250 nm). Hence the EDX shows that the content of K^+ is 0.71 wt% on the whole surface of HWO (Fig. 9b) tested, whereas the total content of K^+ on K-V_2O_5/HWO-C is 1.75 wt% via XRF analysis (Table 1). To sum up, 0.71 wt% K^+ has been located on the HWO-C external surface and 1.04 wt% K^+ has entered into the HWO-C channels according to the semiquantitative analysis.

As a traditional acidity analysis, the desorption temperature in the NH_3-TPD-TCD experiment is always to start about 100 °C to avoid the signal interference, as shown in Fig S3. It can been seen that the peaks located < 220 °C and > 300 °C are assigned to the weak and strong absorbed NH_3 on acid sites, respectively. However the TCD signal can't represent and clarify all gases signals during NH_3 desorption process. Furthermore, in order to measure different gases in the NH_3-TPD process exactly, the online NH_3-TPD-MS is carried out to record the desorption process from the 50 °C to 800 °C. The NH_3-TPD-MS results could be more accurate to distinguish the acid strength and avoid interference caused by the signal peaks of other substances. The NH_3 signals of

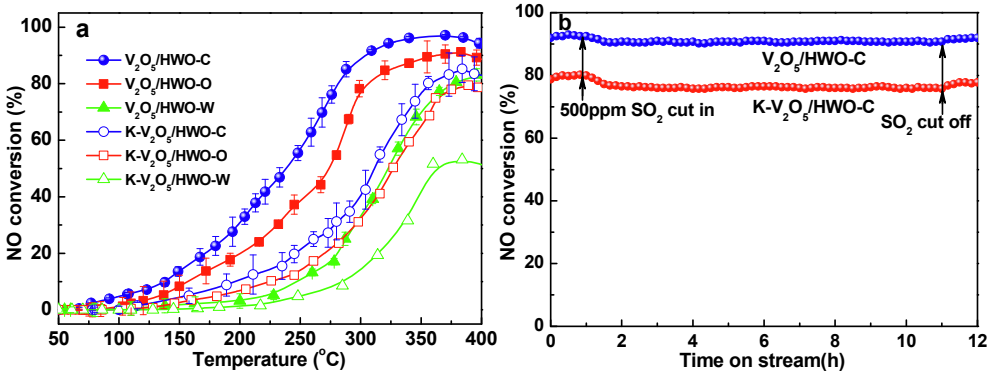

Fig. 12. (a) SCR activity of the catalysts with the reaction condition: [NH_3] = [NO] = 300 ppm, [O_2] = 5 vol%; (b) Effect of SO_2 on the SCR duration tests under the V_2O_5/HWO-C and K-V_2O_5/HWO-C catalysts at 360 °C with the reaction condition: [NH_3] = [NO] = 400 ppm, [O_2] = 5 vol%, [SO_2] = 500 ppm.

catalysts are monitored by the mass spectrometer (Fig. 10a). Correspondingly, the N_2 signal is detected synchronously to evidence that the NH_3 adsorbed on acid sites is thermally desorbed to yield N_2 (Fig. 10b). The large NH_3 chemical desorption curves around 200 °C is contributed to weakly bond NH_3 on the acid sites (Lewis acid) for the catalysts. The two typical medium-temperature desorption peaks of NH_3 (γ and δ) and two remarkable peaks of N_2 (α and β) are found on the V_2O_5/HWO-C catalyst, indicating that the NH_3 bond to strong acid sites (Brønsted acid) on V_2O_5/HWO-C is more easily activated and thermally desorbed to yield N_2 release, and closely attributable to the selective reduction of NO for SCR reaction. Our previous work found that the Brønsted acid sites not only bind and disperse transition metal ions but also absorb and activate ammonia[40,41]. Hence, the role is contradictory because metal ions well dispersed here are unable to bind a significant amount of physisorbed NH_3 on the V_2O_5/HWO-C.

The NO desorption analysis is also carried out to detected the NO and N_2O signals in Fig. 11a and 11b during NO-TPD, assigned to the key step of SCR reaction [42]. The desorption peak of NO centered in the < 200 °C is attributed to the physical desorption of NO bounded to amorphous clusters and well dispersed V_2O_5 oxides, easily absorbed on the some K^+ of the K-V_2O_5/HWO-C surface (Fig. 11a), and another peak at > 200 °C corresponds to the chemical desorption of NO strongly bounded to bulk V_2O_5 oxides. The N_2O curves is measured synchronously at 180–800 °C since the NO is tend to be adsorbed on metal sites, and two N-O bonds are activated to convert into N_2O at elevated temperatures. The remarkable desorption peak area of N_2O is observed (Fig. 11b) at low temperature over V_2O_5/HWO-C, supporting that the relatively weak bond strength between well dispersed vanadium species and NO would facilitate the selective reduction of NO with NH_3, which is similar to the results of the other literatures[43,44].

3.3. SCR activity and resistance to K poisoning

Fig. 12 displays the SCR activity and duration tests for the catalysts to show the catalytic activity and alkali resistance capacity. The V_2O_5/HWO-C catalyst exhibits a higher activity than that of V_2O_5/HWO-W and V_2O_5/HWO-O, reaching a maximum NO conversion of 97 % at 360 °C and > 90 % NO conversion within the wide temperature range of 300–400 °C (Fig. 12a). The excellent activity obtained for V_2O_5/HWO-C can be attributed to the good dispersion of V_2O_5 on the smooth rod-shaped morphology of HWO and the abundant number of active oxygen atoms and acid sites on the catalyst surface, as proven by the XRD, TEM, H_2-TPR and XPS results. After being subjected to a K^+ load, K-V_2O_5/HWO-C exhibits acceptable alkali resistance, with the highest NO conversion reaching 83 % at 360 °C among all the catalysts tested. The good N_2 selectivity below the 400 °C is also obtained in the Fig.S4. The SCR activity and alkali resistance compared to the reported catalysts [25,26,29,39,45] are shown in Table 2. It was reported that the presence

Table 2
The SCR activity over different catalysts under different reaction conditions.

Samples	Reaction gas mixture	GHSV (h^{-1})	Temperature (°C)	X_{NO} (%)	Refs.
V_2O_5/HWO	NO = NH_3 = 500 ppm, 3 vol% O_2, 1,300 mg·m^{-3} SO_2, N_2 balanced	200,000	350	92	[25]
K_2SO_4-V_2O_5/HWO		200,000	350	92	[25]
K_2SO_4-V_2O_5/WO_3-TiO_2		200,000	350	<10	[25]
V_2O_5/HWO	NO = NH_3 = 1000 ppm, 3 vol% O_2, N_2 balanced	80,000	350	90	[26]
V_2O_5/K_{in}HWO		80,000	350	~80	[26]
V_2O_5-S/CeO_2	NO = NH_3 = 500 ppm,5 vol% O_2, N_2 balanced	100,000	350	~98	[29]
K-V_2O_5-S/CeO_2		100,000	350	~95	[29]
K0.1-VWTi	NO = NH_3 = 500 ppm, 3 vol% O_2, N_2 balanced	70,000	350	96	[39]
K1-VWTi		70,000	350	20	[39]
V_2O_5/TiO_2	NO = NH_3 = 500 ppm, 5 vol% O_2, 1,500 ppm SO_2, 5 vol% H_2O, N_2 balanced	8,000	400	95	[45]
K/V(1.3)-Imp-V_2O_5/TiO_2		8,000	400	88	[45]
K/V(1.3)-Dif-V_2O_5/TiO_2		8,000	400	80	[45]
V_2O_5/HWO-C	NH_3 = NO = 300 ppm, O_2 = 5 vol%, N_2 balanced	170,000	360	97	In this work
		170,000	360	83	
K-V_2O_5/HWO-C		170,000	360	90	
		170,000	360	74	
V_2O_5/HWO-O		170,000	360	79	
K-V_2O_5/HWO-O		170,000	360	52	
V_2O_5/HWO-W					
K-V_2O_5/HWO-W					
V_2O_5/HWO-C	NH_3 = NO = 300 ppm, O_2 = 5 vol%, SO_2 = 500 ppm, N_2 balanced	170,000	360	91	In this work
K-V_2O_5/HWO-C		170,000	360	76	
V_2O_5/HWO-O		170,000	360	84	
K-V_2O_5/HWO-O		170,000	360	70	

of SO_2 may have a negative effect on the alkali resistance of V_2O_5-based catalysts [39,10,47]. Hence the influence of SO_2 on SCR stability was tested over the V_2O_5/HWO-C and K-V_2O_5/HWO-C, with the results shown in Fig. 12b. When 500 ppm (1400 mg/m^3) of SO_2 was introduced, the NO conversion for V_2O_5/HWO-C and K-V_2O_5/HWO-C slightly decreased from 93% to 91% and from 80% to 76% respectively, and maintain at such a conversion level for approximate 10 h, which indicate that slight interactions were occurred between alkalis and SO_2 in the SCR process. The activity of V_2O_5/HWO-C and K-V_2O_5/HWO-C recovered to 92% and 78% within 20 min, respectively. Li et al [10] reported that the V_2O_5-based catalysts exhibit a strong SO_2 tolerance and weak alkali resistance performance. Hence the results of SCR stability test convince that effective alkali resistance of the K-V_2O_5/HWO-C originates from the capture of HWO channels, and the slight interactions between alkalis and SO_2 occurs owing to almost 0.71 % K^+ located on the HWO-C external surface. The SEM and NH_3-TPD characterizations of the V_2O_5/HWO-C and K-V_2O_5/HWO-C catalysts after the SCR reaction have been supplied to explore the changes of morphology and acidity, as shown in Fig.S5 and Fig. S6, respectively. It can be found from Fig.S5 that the regular morphology is unchanged although the slight agglomeration on the catalyst surface, exhibiting the good resistance of SO_2. After SO_2-resistaing testing, the peak area becomes smaller and the temperature of peaks transform higher for the used V_2O_5/HWO-C and K-V_2O_5/HWO-C catalyst, indicating that the NH_3 adsorption might become relative weaker on the catalyst surface. A reasonable explanation is that the slight sulfated species occupy adsorption sites and disturb NH_3 adsorption, in agreement with the small activity reduction of the catalysts.

To investigate the SCR reaction mechanism related to K^+ poisoning and trapping, samples for in situ IR analysis were pretreated under a N_2 flow of 100 mL/min with a 10 °C/min heating rate. Adsorption of 5 vol% NH_3/N_2 on V_2O_5/HWO-C (Fig. 13a) leads to the formation of many NH_4^+ species on the BrØnsted acid sites at 1410 cm^{-1} and the absorption of NH_3 on the Lewis acid sites at 1345 cm^{-1} [46,48,49]. In contrast, the Brønsted adsorption on K-V_2O_5/HWO-C (Fig. 13b) nearly disappeared, although the Lewis adsorption was obviously unchanged. The decrease in surface acid sites is induced by the capture of K^+ by HWO channels via the ion exchange pathway (W-O–H + K^+→W-O-K + H^+), in agreement with the XRD and NH_3-TPD results. With the increase of temperature from 50 to 500 °C, the 1345 cm^{-1} peak of catalysts became slightly stronger, which can be attributed to the activated NH_4^+ species and then transform to NH_3 on the catalyst surface. After pre-adsorption of 5 vol% NO + air, absorbed NO (1630 cm^{-1}) and absorbed NO_2 (1600 cm^{-1}) are formed[50,51], and the intensity of the peaks does not change for the V_2O_5 of V_2O_5/HWO-C and K-V_2O_5/HWO-C (Fig. 13c-d). This behaviour confirms that the HWO channels can effectively trap K^+ and prevent K^+ poisoning of V_2O_5. The bands at 1355 and 1300–1140 cm^{-1} are attributed to the chelated nitrite and bidentate nitrate species, respectively. In particular, the peak intensity at 1355 cm^{-1} for K-V_2O_5/HWO-C is higher than that for V_2O_5/HWO-C due to the occurrence of the K-O bond in the catalyst, in agreement with XRD and Rietveld refinements results, and verified by the literatures[23,25]. With a temperature increase to 500 °C, the peaks of absorbed NO and absorbed NO_2 decrease first, followed by the peaks of nitrite and nitrate species. Similar spectra are observed for V_2O_5/HWO-C (Fig. '13e) and K-V_2O_5/HWO-C (Fig. 13f). The bands at 1513 and 1413 cm^{-1} (NH_4^+ species on the BrØnsted acid sites), 1340 cm^{-1} (NH_3 on the Lewis acid sites), 1626 cm^{-1} (absorbed NO), and 1300–1140 cm^{-1} (chelated nitrite and bidentate nitrate species) are observed. However, the band at 1413 cm^{-1} of K-V_2O_5/HWO-C is weaker than that of V_2O_5/HWO-C under 5 vol% NH_3 + 5 vol% NO + air pre-adsorption because of the slight K^+ poisoning. With the temperature increasing (50–500 °C), a series of NO_x species including NO_{abs},

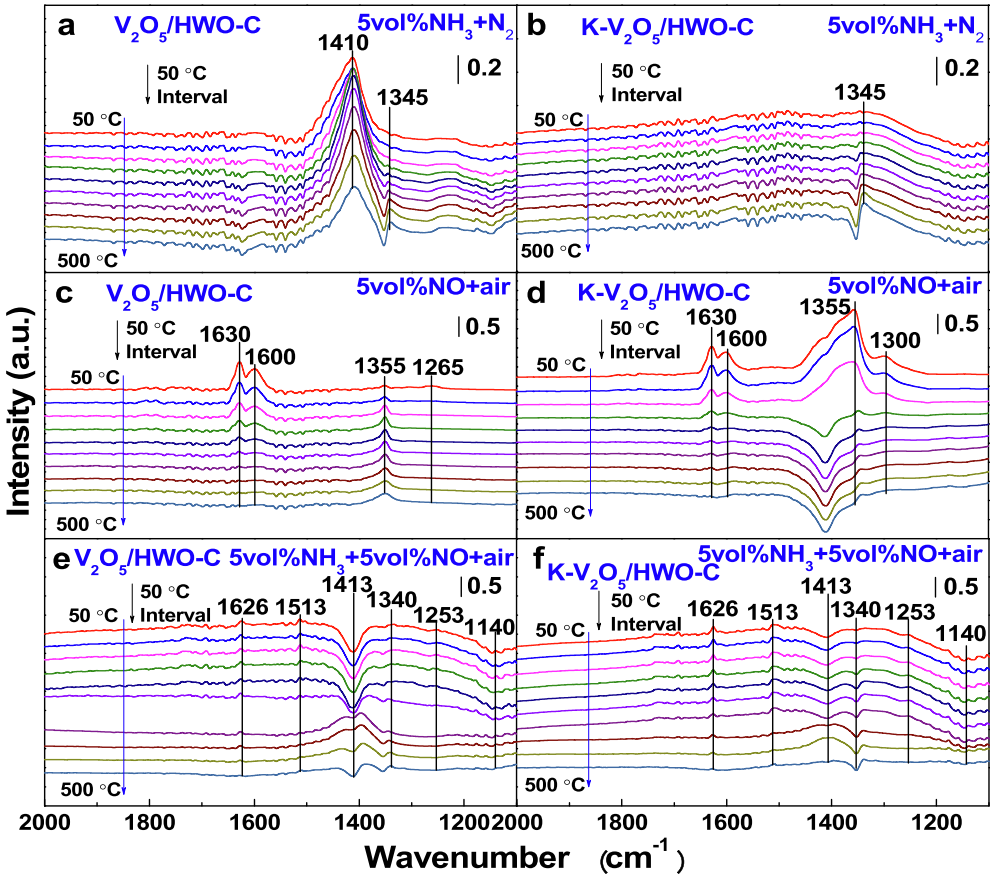

Fig. 13. In situ IR spectra of V_2O_5/HWO-C and K-V_2O_5/HWO-C (50–500 °C) under different pre-adsorption conditions.

NO_{2abs}, NO_2^- and NO_3^- are formed via NO + O_2 at the V_2O_5 sites, which react with the NH_4^+ (BrØnsted) and NH_{3abs} (Lewis) groups of V_2O_5 and HWO sites to release N_2 and H_2O, following the Langmuir-Hinshelwood (L-H) mechanism.

3.4. K Resistance mechanism for the SCR reaction

According to the analysis above, the excellent activity obtained for V_2O_5/HWO-C can be attributed to the well dispersed V_2O_5 on the smooth rod-shaped morphology of HWO and the abundant number of active oxygen atoms and acid sites on the catalyst surface. The proposed K resistance mechanism and detailed pathways of intermediates for the SCR reaction are shown in Fig. 14. Combined with the IR results, a series of NO_x species including NO_{abs}, NO_{2abs}, NO_2^- and NO_3^- are formed via NO + O_2 at the V_2O_5 sites, which react with the NH_4^+ (BrØnsted) and NH_{3abs} (Lewis) groups of V_2O_5 and HWO to release N_2 and H_2O, following the L-H mechanism (Fig. 14a and Fig. 14d), verified by the Zhu et al [52]. Most K^+ (approximately 1.04 wt%) can be effectively captured in the smooth rod-shaped HWO-C channels with via the ion exchange pathway (Fig. 14c and Fig. 14d), because the K^+ ions inatially react with protons of HWO-C via ion exchange, and then are stably fixed at the alkali-trapping sites via the coordination with the oxgen atoms of the cavities (W-O–H + K^+→W-O-K + H^+), concomitant with an energy saving [8,23]. Therefore, the V_2O_5/HWO-C can realize effective resistance of K poisoning via the coordination of the two sites: one is the alkali capture sites of HWO, and the other is the active sites of V_2O_5 on the catalyst. And the rest of K^+ ions (approximately 0.71 wt%) are located on the HWO-C external surface via weak bonds to V_2O_5, resulting in a decrease in the number of BrØnsted acid sites and some degree of alkali poisoning (Fig. 14b and Fig. 14d), which is in agreement with the SCR activity results. In this case, the coordination of the two sites is effectively realized for resisting K poisoning via the active sites of V_2O_5 and the K capture sites of HWO-C channels on the K-V_2O_5/HWO-C catalyst.

4. Conclusions

The V_2O_5/HWO catalysts are synthesized using different pore-forming agents for the SCR of NO with NH_3. The catalytic activity for SCR decreases in the order of V_2O_5/HWO-C > V_2O_5/HWO-O > V_2O_5/HWO-W, which is due to the highly dispersed V_2O_5, high specific surface area, abundant amounts of active oxygen, surface acidity, and smooth rod-shaped morphology of HWO in the V_2O_5/HWO-C catalyst. The obtained results provide evidence that commercial bacterial cellulose achieves controllable synthesis to form catalysts with a regular morphology. The V_2O_5/HWO-C catalyst exhibits a relative effective resistance of alkali and SO_2. The NO_x intermediate species including NO_{abs}, NO_{2abs}, NO_2^- and NO_3^- are formed on the V_2O_5 active sites and react with the NH_4^+ and NH_{3abs} groups of V_2O_5 and HWO, mainly following the L-H mechanism during the SCR reaction. After being subjected to a K^+ load, V_2O_5/HWO-C effectively resisted K poisoning via the coordination of the two sites, where most of the K^+ ions (1.04 wt%) can be effectively captured in the HWO-C channels with K-O bond, and a slight amount of K^+ (0.71 wt%) is located on the HWO-C external surface and forms weak bonds with V_2O_5.

CRediT authorship contribution statement

Running Kang: Data curation, Formal analysis, Investigation, Writing - original draft, Writing - review & editing. **Junyao He:** Data curation, Formal analysis. **Feng Bin:** Formal analysis, Methodology, Supervision, Validation, Writing - review & editing. **Baojuan Dou:** Methodology, Validation. **Qinglan Hao:** Methodology, Resources,

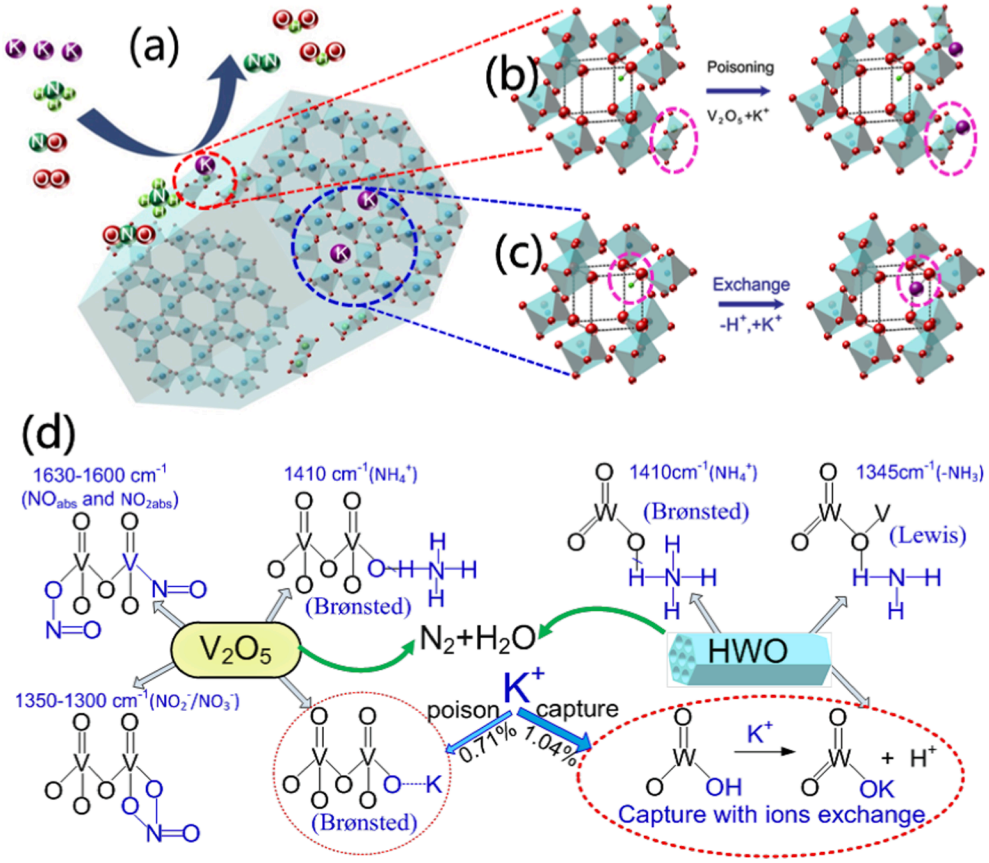

Fig. 14. Schematic model of the K-V_2O_5/HWO-C catalyst: (a) SCR reaction mechanism with alkali metals, (b) slight alkali poisoning with V_2O_5 on the surface, (c) alkali resistance by HWO channel capture, and (d) detailed pathways of intermediates and forms of K^+.

Validation. **Xiaolin Wei:** Funding acquisition, Project administration, Supervision. **Kwun Nam Hui:** Methodology, Writing - review & editing. **Kwan San Hui:** Methodology, Validation, Writing - review & editing.

Declaration of Competing Interest

The authors declare that they have no known competing financial interests or personal relationships that could have appeared to influence the work reported in this paper.

Acknowledgements

We sincerely thank Prof. Lv Gang (Tianjin University) for the help and reasonable suggestions about SCR reaction mechanism. We gratefully acknowledge the financial support from the National Natural Science Foundation of China (No. 51736010), and the Key Projects of Tianjin Natural Science Foundation (19JCZDJC40100).

Appendix A. Supplementary data

Supplementary data to this article can be found online at https://doi.org/10.1016/j.fuel.2021.121445.

References

[1] Pan YJ, Shen BX, Liu LJ, Yao Y, Gao HP, Liang C, et al. Develop high efficient of NH_3-SCR catalysts with wide temperature range by ball-milled method. Fuel 2020;282:118834.
[2] Lai JK, Wachs IE. A perspective on the selective catalytic reduction (SCR) of NO with NH_3 by supported V_2O_5−WO_3/TiO_2 Catalysts. ACS Catal 2018;8:6537–51.
[3] Hou Y, Wang J, Li Q, Liu Y, Bai Y, Zeng Z, et al. Environmental-friendly production of FeNbTi catalyst with significant enhancement in SCR activity and SO_2 resistance for NO_x removal. Fuel 2021;285:119133. https://doi.org/10.1016/j.fuel.2020.119133.
[4] Inomata Y, Kubota H, Hata S, Kiyonaga E, Morita K, Yoshida K, et al. Bulk tungsten-substituted vanadium oxide for lowtemperature NOx removal in the presence of water. Nat Commun 2021;12(1). https://doi.org/10.1038/s41467-020-20867-w.
[5] Strege JR, Zygarlicke CJ, Folkedahl BC, McCollor DP. SCR deactivation in a full-scale cofire-utility boiler. Fuel 2008;87(7):1341–7.
[6] Nicosia D, Czekaj I, Krocher O. Chemical deactivation of V_2O_5/WO_3-TiO_2 SCR catalysts by additives and impurities from fuels lubrication oils and urea solution Characterization study of the effect of alkali and alkaline earth metals. Appl. Catal., B: Environ. 2008;77:228–36.
[7] Zhang SL, Zhong Q. Surface characterization studies on the interaction of V_2O_5–WO_3/TiO_2 catalyst for low temperature SCR of NO with NH_3. J Solid State Chem 2015;221:49–56.
[8] Huang ZW, Gu X, Wen W, Hu PP, Makkee M, Lin H, et al. A “smart” hollandite $deNO_x$ catalyst: self-protection against alkali poisoning. Angew Chem Int Ed 2013;320(52):660–4.
[9] Wang XX, Cong QL, Chen L, Shi Y, Shi Y, Li SJ, et al. The alkali resistance of CuNbTi catalyst for selective reduction of NO by NH_3: A comparative investigation with VWTi catalyst. Appl. Catal. B: Environ. 2019;246:166–79.
[10] Li Q, Chen S, Liu Z, Liu Q. Combined effect of KCl and SO_2 on the selective catalytic reduction of NO by NH_3 over V_2O_5/TiO_2 catalyst. Appl Catal B Environ 2015;164:475–82.
[11] Cai S, Xu T, Wang P, Han L, Impeng S, Li Y, et al. Self-Protected CeO_2–SnO_2@SO_4^{2-}/TiO_2 Catalysts with Extraordinary Resistance to Alkali and Heavy Metals for NOx Reduction. Environ Sci Technol 2020;54(19):12752–60.
[12] Yan L, Ji Y, Wang P, Feng C, Han L, Li H, et al. Alkali and Phosphorus Resistant Zeolite-like Catalysts for NO_x Reduction by NH_3. Environ Sci Technol 2020;54(14):9132–41.
[13] Wang P, Yan L, Gu Y, Kuboon S, Li H, Yan T, et al. Poisoning-Resistant NO_x Reduction in the Presence of Alkaline and Heavy Metals over H-SAPO-34-Supported Ce-Promoted Cu-Based Catalysts. Environ Sci Technol 2020;54(10):6396–405.
[14] Yang J, Tang W, Liu X, Chao C, Liu J, Sun D. Bacterial cellulose-assisted hydrothermal synthesis and catalytic performance of La_2CuO_4 nanofiber for methanol steam reforming. In. J Hydrogen. Energ. 2013;38(25):10813–8.
[15] Wu X, Yu W, Si Z, Weng D. Chemical deactivation of V_2O_5-WO_3/TiO_2 SCR catalyst by combined effect of potassium and chloride. Front Environ Sci Eng 2013;7:420–7.
[16] Lian ZH, Li YJ, Shan WP, He H. Recent progress on improving low-temperature activity of vanadia-based catalysts for the selective catalytic reduction of NO_x with ammonia. Catalysts 2020;10(1421):1–19.
[17] Lian ZH, Deng H, Xin SH, Shan WP, Wang Q, Xu J, et al. Significant promotion effect of rutile phase on V_2O_5/TiO_2 catalyst for NH_3-SCR. Chem Commun 2020. https://doi.org/10.1039/D0CC05938B.
[18] Deng L, Liu X, Cao PQ, Zhao YG, Du YB, Wang CA, et al. A study on deactivation of V_2O_5-WO_3-TiO_2 SCR catalyst by alkali metals during entrained-flow combustion. J Energy Inst 2017;90:743–51.
[19] Kong M, Liu QC, Zhou J, Jiang LJ, Tian YM, Yang J, et al. Effect of different potassium species on the deactivation of V_2O_5-WO_3-TiO_2 SCR catalyst: Comparison of K_2SO_4, KCl and K_2O. Chem Eng J 2018;348:637–43.
[20] Li J, Peng Y, Chang H, Li X, Crittenden JC, Hao J. Chemical poisoning and regeneration of SCR catalysts for NO_x removal from stationary sources. Front. Environ. Sci. Eng. 2016;10:413–27.
[21] He Y, Ford ME, Zhu M, Tumuluri QU, Wu LZ, Wachs IE. Influence of catalyst synthesis method on selective catalytic reduction (SCR) of NO by NH_3 with V_2O_5-WO_3-TiO_2 catalysts. Appl Catal B Environ 2016;193:141–50.
[22] Kwon DW, Park KH, Hong SC. The influence on SCR activity of the atomic structure of V_2O_5/TiO_2 catalysts prepared by a mechanochemical method. Appl Catal A General 2013;451:227–35.
[23] Hu PP, Huang ZW, Gu X, Xu F, Gao J, Wang Y, et al. Alkali-resistant mechanism of a hollandite $DeNO_x$ catalyst. Environ Sci Technol 2015;49:7042–7.
[24] Zhou G, Maitarad P, Wang P, Han L, Yan T, Li H, et al. Alkali-Resistant NO_x Reduction over SCR Catalysts via Boosting NH_3 Adsorption Rates by In Situ Constructing the Sacrificed Sites. Environ Sci Technol 2020;54(20):13314–21.
[25] Huang ZW, Li H, Gao JY, Gu X, Zheng L, Hu PP, et al. Alkali- and sulfur-resistant tungsten-based catalysts for NO_x emissions control. Environ Sci Technol 2015;49:14460–5.
[26] Zheng Li, Zhou M, Huang Z, Chen Y, Gao J, Ma Z, et al. Self-protection mechanism of hexagonal WO_3-based $DeNO_x$ catalysts against alkali poisoning. Environ Sci Technol 2016;50(21):11951–6.
[27] Wan Q, Duan L, Li JH, Chen L, He KB, Hao JM. Deactivation performance and mechanism of alkali (earth) metals on V_2O_5–WO_3/TiO_2 catalyst for oxidation of gaseous elemental mercury in simulated coal-fired flue gas. Catal Today 2011;175:189–95.
[28] Li SW, Xu Y, Chen YF, Li WZ, Lin LL, Li MZ, et al. Tuning the selectivity of catalytic carbon dioxide hydrogenation over Iridium/Cerium oxide catalysts with a strong metal-support interaction. Angew Chem Int Ed 2017;56:10761–5.
[29] Zhou GY, Maitarad P, Wang PL, Han LP, Yan TT, Li HR, et al. Alkali-Resistant NO_x Reduction over SCR Catalysts via Boosting NH_3 Adsorption Rates by In Situ Constructing the Sacrificed Sites. Environ Sci Technol 2020;54(20):13314–21.
[30] Shannon RD. Revised effective ionic radii and systematic studies of interatomic distances in halides and chalcogenides. Acta Crystallogr A 1976;32(5):751–67.
[31] Chen Li, Lam S, Zeng Q, Amal R, Yu A. Effect of cation intercalation on the growth of hexagonal WO_3 nanorods. J Phys Chem C 2012;116(21):11722–7.
[32] Zhu N, Shan WP, Lian ZH, Zhang Y, Liu K, He H. A superior Fe-V-Ti catalyst with high activity and SO_2 resistance for the selective catalytic reduction of NO_x with NH_3. J Hazard Mater 2020;382. https://doi.org/10.1016/j.jhazmat.2019.120970.
[33] Zhang SL, Zhong Q. Promotional effect of WO_3 on O^{2-} over V_2O_5/TiO_2 catalyst for selective catalytic reduction of NO with NH_3. J. Mol. Catal. A-Chem. 2013;373:108–13.
[34] Chen JP, Yang RT. Role of WO_3 in mixed V_2O_5–WO_3/TiO_2 catalysts for selective catalytic reduction of nitric oxide with ammonia. Appl. Catal. A. Gen. 1992;80(1):135–48.
[35] Shi J-W, Wang Y, Duan R, Gao C, Wang B, He C, et al. The synergistic effects between Ce and Cu in $Cu_yCe_{1-y}W_5O_x$ catalysts for enhanced NH_3-SCR of NO_x and SO_2 tolerance. Catal Sci Technol 2019;9(3):718–30.
[36] Wang D, Peng Y, Xiong S-C, Li B, Gan L-n, Lu C-M, et al. De-reducibility mechanism of titanium on maghemite catalysts for the SCR reaction: An in situ DRIFTS and quantitative kinetics study. Appl Catal B Environ 2018;221:556–64.
[37] Huang J, Teng Z, Kang R, Bin F, Wei X, Hao Q, et al. Study on activity, stability limit and reaction mechanism of CO self-sustained combustion over the $LaMnO_3$, $La_{0.9}Ce_{0.1}MnO_3$ and $La_{0.9}Sr_{0.1}MnO_3$ perovskite catalysts using sugar agent. Fuel 2021;292:120289. https://doi.org/10.1016/j.fuel.2021.120289.
[38] Reiche MA, Maciejewski M, Baiker A. Characterization by temperature programmed reduction. Catal Today 2000;56(4):347–55.
[39] Chen L, Li JH, Ge MF. The poisoning effect of alkali metals doping over nano $_V2_O5$–W_O3/Ti_O2 catalysts on selective catalytic reduction of N_Ox by N_H3. Chem Eng J 2011;170:531–7.
[40] Bin F, Song C, Lv G, Song J, Cao X, Pang H, et al. Structural characterization and selective catalytic reduction of nitrogen oxides with ammonia: a comparison between Co/ZSM-5 and Co/SBA-15. J Phys Chem C 2012;116:26262–74.
[41] Bin F, Song C, Lv G, Song J, Wu S, Li X. Selective catalytic reduction of nitric oxide with ammonia over zirconium-doped copper/ZSM-5 catalysts. Appl Catal B Environ 2014;150–151:532–43.
[42] Zhong L, Cai W, Yu Y, Zhong Q. Insights into synergistic effect of chromium oxides and ceria supported on Ti-PILC for NO oxidation and their surface species study. Appl Sur Sci 2015;325:52–63.
[43] TopsØe NY, TopsØe H, Dumesic JA. Vanadia/titania catalysts for selective catalytic reduction (SCR) of nitric oxide by ammonia. J Catal 1995;151:226–40.
[44] Lietti L. Reactivity of V_2O_5-WO_3/TiO_2 de-$NO_{(x)}$ catalysts by transient methods. Appl Catal B Environ 1996;10:281–97.
[45] Lei TY, Li QC, Chen SF, Liu ZY, Liu QY. KCl-induced deactivation of V_2O_5–WO_3/TiO_2 catalyst during selective catalytic reduction of NO by NH_3: Comparison of poisoning methods. Chem Eng J 2016;296:1–10.
[46] Guo R-T, Wang S-X, Pan W-G, Li M-Y, Sun P, Liu S-M, et al. Different poisoning effects of K and Mg on the Mn/TiO_2 catalyst for selective catalytic reduction of NOx with NH_3: A Mechanistic Study. J. Liu. J. Phys. Chem. C. 2017;121(14):7881–91.
[47] Chen J, Yang RT. Mechanism of Poisoning of the V_2O_5/TiO_2 Catalyst for the Reduction of NO by NH_3. J Catal 1990;125:411–20.

[48] Hu WS, Zhang YH, Liu SJ, Zheng CH, Xiang Gao I, Nova ET. Improvement in activity and alkali resistance of a novel V-Ce$(SO_4)_2$/Ti catalyst for selective catalytic reduction of NO with NH_3. Appl Catal B Environ 2017;206:449–60.
[49] Rasmussen SB, Portela R, Bazin P, Ávila P, Bañares MA, Daturi M. Transient operando study on the NH_3/NH_4^+ interplay in V-SCR monolithic catalysts. Appl Catal B Environ 2018;224:109–15.
[50] Marberger A, Ferri D, Elsener M, Krocher O. The significance of lewis acid sites for the selective catalytic reduction of nitric oxide on vanadium-based catalysts. Angew Chem Int Ed 2016;55:11989–94.
[51] Hadjiivanov K, Concepcion P. Analysis of oxidation states of vanadium in vanadia−titania catalysts by the IR spectra of adsorbed NO. Top Catal 2000;12:123–30.
[52] Zhu M, Lai JK, Tumuluri U, Ford ME, Wu Z, Wachs IE. Reaction pathways and kinetics for selective catalytic reduction (SCR) of acidic NO_x emissions from power plants with NH_3. ACS Catal 2017;7:8358–61.